Minimizing residues and strain in 2D materials transferred from PDMS

OPEN ACCESS
IOP Publishing
Nanotechnology

Nanotechnology **29** (2018) 265203 (9pp)
https://doi.org/10.1088/1361-6528/aabd90

Minimizing residues and strain in 2D materials transferred from PDMS

Achint Jain[1], Palash Bharadwaj[2], Sebastian Heeg[1], Markus Parzefall[1], Takashi Taniguchi[3], Kenji Watanabe[3] and Lukas Novotny[1]

[1] Photonics Laboratory, ETH Zürich, 8093 Zürich, Switzerland
[2] Department of Electrical and Computer Engineering, Rice University, Houston, TX 77005, United States of America
[3] National Institute for Material Science, 1-1 Namiki, Tsukuba 305-0044, Japan

E-mail: lnovotny@ethz.ch

Received 9 February 2018, revised 29 March 2018
Accepted for publication 12 April 2018
Published 3 May 2018

Abstract

Integrating layered two-dimensional (2D) materials into 3D heterostructures offers opportunities for novel material functionalities and applications in electronics and photonics. In order to build the highest quality heterostructures, it is crucial to preserve the cleanliness and morphology of 2D material surfaces that come in contact with polymers such as PDMS during transfer. Here we report that substantial residues and up to ~0.22% compressive strain can be present in monolayer MoS_2 transferred using PDMS. We show that a UV-ozone pre-cleaning of the PDMS surface before exfoliation significantly reduces organic residues on transferred MoS_2 flakes. An additional 200 °C vacuum anneal after transfer efficiently removes interfacial bubbles and wrinkles as well as accumulated strain, thereby restoring the surface morphology of transferred flakes to their native state. Our recipe is important for building clean heterostructures of 2D materials and increasing the reproducibility and reliability of devices based on them.

Supplementary material for this article is available online

Keywords: TMDCs, van der Waals heterostructures, transfer techniques, material synthesis strain

(Some figures may appear in colour only in the online journal)

1. Introduction

Two-dimensional (2D) materials like graphene, hexagonal boron nitride (hBN), transition metal dichalcogenides (TMDCs), etc., have gained immense attention in recent years due to the wealth of novel fundamental properties and fascinating physical phenomena exhibited by them [1, 2]. A unique possibility existing with these materials is that of assembling them into 3D heterostructures to create artificial materials which do not exist naturally and thus give rise to new functionalities which seem promising for many future applications [3, 4]. These heterostructures can be built by a variety of methods [5] like chemical vapor deposition (CVD) [6], epitaxial growth [7, 8], inkjet printing [9] or more generally by mechanical stacking of individual layers [10, 11]. Among the many available techniques for stacking 2D materials [11–16], one approach that has become common recently is to mechanically exfoliate bulk 2D crystals onto a stamp made of a viscoelastic material, such as poly-dimethylsiloxane (PDMS), bring them in contact with a desired substrate and then slowly detach the stamp to leave the 2D flakes behind [17, 18]. Although this procedure is very versatile, deterministic and fairly simple to perform, not much attention has been paid to the surface cleanliness of the flakes transferred this way.

PDMS is a widely used polymer for contact printing [19], microfluidics [20] as well as stretchable electronics [21], and

its chemistry has been studied extensively [22]. PDMS is composed of a network of cross-linked dimethylsiloxane oligomers which do not get fully cross-linked even after extensive curing [23] and depending on the curing time and temperature, up to 5% of oligomers can remain uncrosslinked within the PDMS bulk [23, 24]. It is well-known that these uncrosslinked species are even present on the surface of PDMS stamps and get transferred to the target substrate during contact printing [25, 26], thereafter acting as a surface contamination layer. PDMS oligomer residues have been characterized previously by many techniques such as non-linear spectroscopy [27], x-ray photoelectron spectroscopy [25, 28], atomic force microscopy (AFM) and ToF-SIMS [28], confirming that PDMS can indeed degrade the surface cleanliness of transferred materials. Residues were also found to occur on 2D materials, e.g. graphene [29] and TMDCs [30], transferred using PDMS. Owing to their 2D structure, the properties of 2D materials are quite sensitive to surface contaminants and residues trapped at the interfaces within 3D heterostructures [31]. Hence, it is essential to stack these materials with minimum residues.

In this work, the cleanliness of 2D materials transferred using PDMS was investigated with the help of AFM and photoluminescence (PL) measurements. Using monolayer (1L) MoS_2 as a test layer, we show evidence for substantial residues being present on MoS_2 transferred onto hBN from PDMS. For transferring MoS_2 in a cleaner way, we developed an ultraviolet-ozone (UV-O_3) treatment recipe to clean the PDMS surface before exfoliating MoS_2 on it and found a significant reduction in residues compared to transfer from untreated PDMS. Using PL and Raman spectroscopy, we further reveal that a small compressive strain can be present in MoS_2 after transfer from PDMS. We found that subsequent vacuum annealing leads to an almost pristine MoS_2 surface on hBN, mostly free from interfacial bubbles, wrinkles and strain. Although here we chose 1L-MoS_2 for demonstration since its sensitive PL and Raman signals allow for systematic optical characterization, our cleaning recipe is general and can be used with other 2D materials as well.

2. Results and discussion

Naturally occurring MoS_2 crystals purchased from SPI Supplies were exfoliated on commercial PDMS films (Gel-Film® PF-40-X4 sold by Gel-Pak) using a blue tape (BT-150E-KL). Figure 1(a) is an optical microscope image of a monolayer MoS_2 flake on PDMS. Bulk hBN crystals were separately exfoliated on O_2 plasma cleaned p^+Si/SiO_2 (285 nm) substrates. The PDMS stamp with MoS_2 was placed on a transparent quartz plate and aligned on top of a suitable hBN flake on SiO_2 using a mask aligner as depicted schematically in figure 1(b). Upon slowly bringing MoS_2 in contact with hBN at room temperature, the entire stack was heated to ∼65 °C for two minutes using a Peltier module kept underneath the Si/SiO_2 substrate. After allowing the stack to cool down, the PDMS stamp was slowly detached as described in [18], leaving behind the MoS_2 flake on hBN (figure 1(c)).

To characterize the surface of the flakes after transfer, we performed topography mapping using an AFM operating in tapping mode. Figure 1(d) shows an AFM topography map of the region outlined in black in figure 1(c). The MoS_2 flake appears mostly 'clean' on this large scale apart from the usual wrinkles and bubbles which are frequently seen in PDMS transferred flakes [18]. However, if we examine the region outlined in red more closely in the higher resolution map in figure 1(e), a dense network of residue islands is clearly visible on the entire MoS_2 surface, making it difficult to even obtain an accurate estimate of the 1L-MoS_2 thickness from a horizontal cross-section (figure 1(h)). Note that these ±0.6 nm (rms) variations in topography cannot arise from substrate roughness alone as the hBN layer below is atomically smooth. Moreover, on the narrower 1L-MoS_2 flake on the right in figure 1(d), a thick residue layer can be clearly identified which is unmistakably distinct from the MoS_2 flake itself. Better visible in the higher resolution AFM map in figure 1(f), this additional layer left-over by PDMS can be as thick as ∼2.5 nm in some areas (magenta profile in figure 1(i)). Together with the topography map in figure 1(e), we also recorded the corresponding AFM phase map as shown in figure 1(g) and observed a poor phase contrast between the MoS_2 and hBN surfaces which also indicates the presence of PDMS residues everywhere.

We tested several flakes and similar residues were found on all of them (see supplementary figure S1 available online at stacks.iop.org/NANO/29/265203/mmedia for residues present on another flake). The amount of residues transferred was also affected by the temperature and pressure applied during the transfer. In case of transfers done without applying any heat, residues were visible even in an optical microscope due a change in the color of the SiO_2 (285 nm) layer which arises from interference and is sensitive to a few nanometers thick transparent organic layer on top (see supplementary figure S2). These results unambiguously demonstrate, in agreement with previous reports [25–30], that PDMS can indeed leave a significant amount of residues behind and an efficient method for eliminating them is genuinely needed.

Although a high temperature (400 °C) vacuum anneal after transfer has been reported to reduce PDMS residues on graphene [29], such high temperatures are known to introduce additional defects in TMDCs [32, 33] which are more fragile compared to graphene. Moreover, we found that annealing by itself is not sufficient to fully restore the transferred flakes to their pristine state. The MoS_2 flake shown in figure 1(c) was annealed at 200 °C in vacuum for 3 h. In the AFM maps in figures 2(a), (b) it can be noticed that although bubbles and wrinkles are mostly gone, the MoS_2 surface is still smeared with residues. This is also evident from the AFM cross-section in figure 2(b) revealing the total thickness of the flake to be 1.6 nm, which is significantly higher than the expected value of 0.7 nm for monolayer MoS_2. An additional vacuum anneal using the same parameters did somewhat reduce the thickness to ∼0.9 nm as depicted in figure 2(c). However, it can be easily seen that the surface topography is quite inhomogeneous and does not approach the cleanliness level of a freshly exfoliated MoS_2 flake.

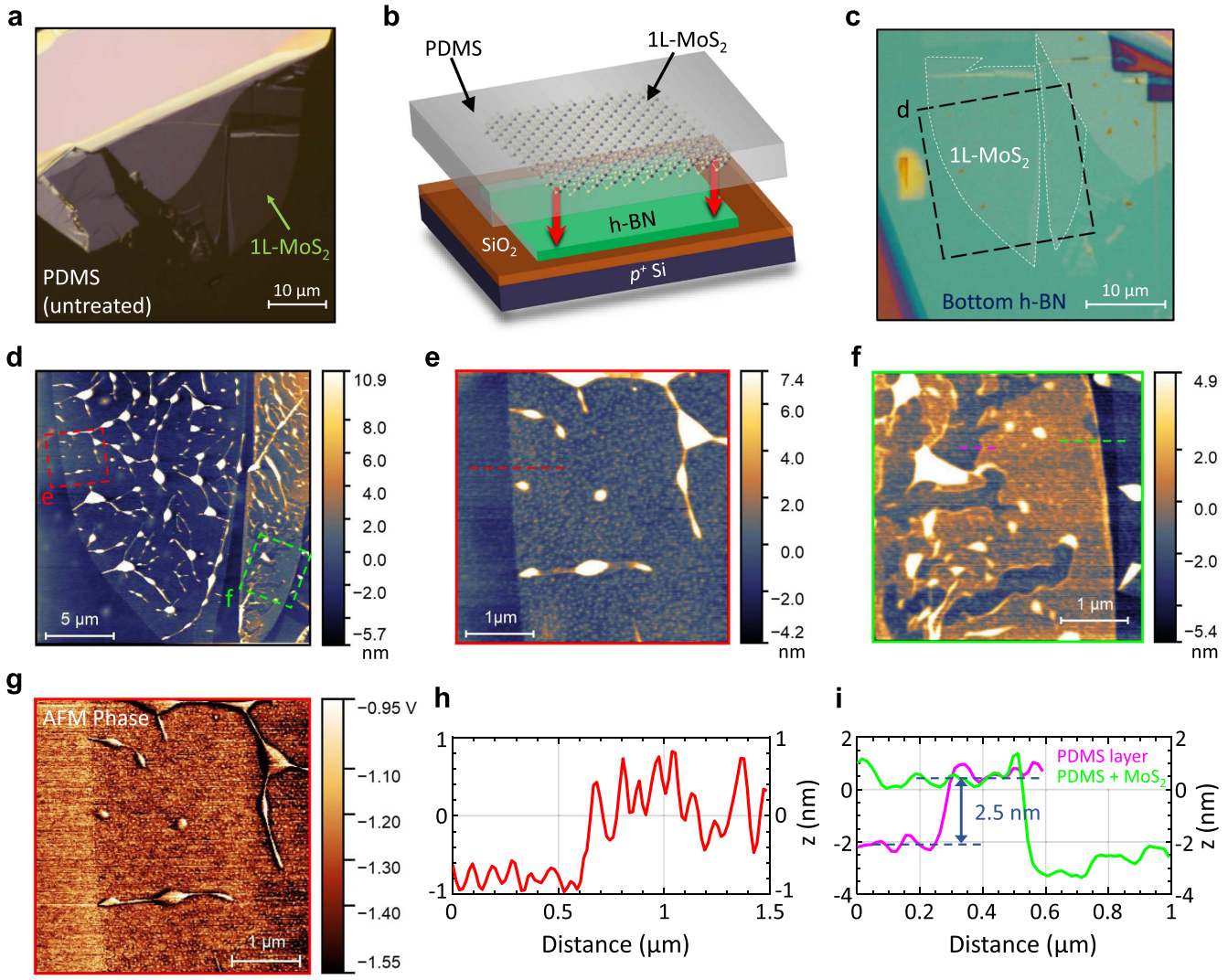

Figure 1. Characterization of PDMS residues. (a) Optical microscope image of a 1L-MoS_2 flake exfoliated on PDMS. (b) Schematic illustration of an inverted PDMS stamp with MoS_2 being transferred onto hBN. (c) The same MoS_2 flake as in (a) after transfer to hBN. (d) Large area AFM topography map of the region outlined in (c) displaying an 'apparently clean' surface together with some bubbles and wrinkles. (e) Higher resolution AFM map of the red-outlined region in (d) exhibiting a dense distribution of residues over the entire MoS_2 flake. (f) Higher resolution AFM map of the green-outlined region in (d) with a thick layer of residues covering a majority of the area. (g) AFM phase map recorded together with the topography in (e) depicting a poor phase contrast between MoS_2 and hBN due to PDMS residues on both surfaces. (h) Height profile across the MoS_2 edge along the dashed line marked in (e). An accurate estimation of the thickness of monolayer MoS_2 is hindered by topography variations due to surface residues. (i) Height profile across the PDMS residue layer and PDMS + MoS_2 along the dashed lines marked in (f). The thickness of the residue layer is ~2.5 nm.

Alternatively, dissolving PDMS residues in organic solvents such as dichloromethane and toluene [24] is also not very effective as the solvent molecules themselves tend to get adsorbed at exposed 2D material surfaces/edges and can even chemically dope TMDCs [34]. This brings us to the question of how to eliminate PDMS residues in a way that does not compromise the 2D material being transferred in any way. In this regard, it appears more reasonable to clean the PDMS surface itself before it comes in contact with the 2D material.

To achieve this, we developed a UV-O_3 treatment recipe to modify the PDMS surface prior to MoS_2 exfoliation. This recipe was found to significantly reduce transfer residues without having any negative effect on the MoS_2. UV-O_3 cleaning of PDMS has been proposed in the past [25] and the mechanism behind it can be understood as follows. Oxygen free radicals and ozone (O_3) created from atmospheric oxygen in the presence of UV-radiation, break down organic species on the PDMS surface into CO_2, H_2O and simpler volatile organic products. At the same time, the silicon present in PDMS gets oxidized and forms a thin (20–30 nm) layer of silicon oxide (SiO_x) on PDMS [35]. This SiO_x surface layer besides having a low carbon content, also acts as a diffusion barrier for uncrosslinked oligomers still present within the PDMS bulk.

To optimize the treatment time, we exposed several PDMS stamps to UV-O_3 in a Bioforce Nanosciences UV Ozone ProCleaner for varying times, and found a duration of 30–40 min to be the optimum. Shorter times did not fully clean the PDMS and longer exposure led to a poorer coverage of flakes on the PDMS upon exfoliation. We also observed that if the exfoliation was done immediately after UV-O_3

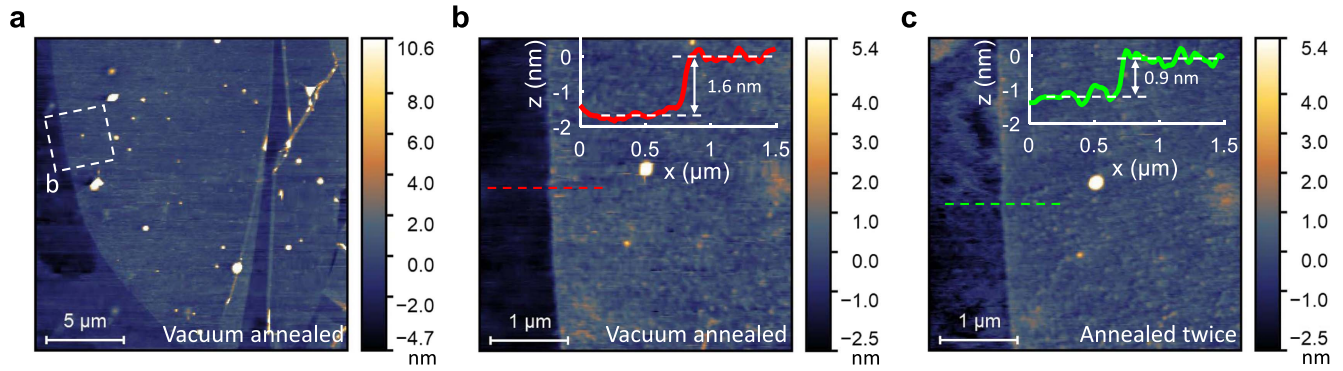

Figure 2. Limited effect of annealing on PDMS residues. (a) AFM topography map of the dirty 1L-MoS_2 flake shown in figure 1(d) after 3 h annealing in vacuum. (b) Higher resolution AFM map of the white-outlined region in (a). Even though the surface appears mostly free from bubbles and more homogeneous than before (see figure 1(e)), a thin layer of PDMS residues is still present over the entire MoS_2 flake. Inset: height profile along the red-dashed line revealing a total thickness of 1.6 nm for the monolayer flake. (d) AFM map of the same region after annealing again for 3 h. Although the total amount of residues does decrease after prolonged annealing, the surface looks far from pristine. Inset: height profile along the green dashed line.

treatment, bonding often occurred between the PDMS and the blue tape used for exfoliation or in rare cases even between the PDMS and O_2 plasma treated SiO_2 surface during the transfer process. However, this bonding could be avoided by leaving the PDMS exposed to ambient air for a few hours to let the surface undergo a partial hydrophobic recovery [36, 37]. This led us to the following optimized process flow, the results of which are presented below.

The PDMS stamp was exposed to UV-O_3 for 30 min and then after a wait interval of 2 h in air, MoS_2 was exfoliated on PDMS as usual. Upon optical identification of suitable flakes, transfer was carried out the same way as described earlier. Figure 3(a) shows an optical microscope image of a large MoS_2 flake exfoliated on 30 min UV-O_3 treated PDMS which was subsequently transferred to hBN (figure 3(b)). In the AFM topography map of the 1L region shown in figure 3(c), one can notice the absence of dense islands or thick layers of PDMS residues unlike in figures 1(e) or (f). Although small amounts of residues can still be detected, this MoS_2 flake is significantly cleaner than the one in figure 1 which was transferred from untreated PDMS (also see supplementary figure S3 for better resolved AFM images of another clean MoS_2 flake).

The large number of bright spots in figure 3(c) are wrinkles and bubbles filled mainly with air molecules and organic adsorbates that become trapped between MoS_2 and hBN during transfer and get squeezed into small pockets via a self-cleaning effect [13, 38]. The amount of trapped bubbles can be reduced by performing the exfoliation and transfer inside an Ar filled glove box to exclude molecular adsorbates [39] or even fully eliminated by stacking in vacuum as shown recently [40]. Alternatively, we found that bubbles and wrinkles can be very efficiently removed by vacuum annealing at 200 °C, similar to another recent report [41]. At this temperature and under low pressure, the trapped species inside the bubbles become mobile and coalesce into bigger bubbles to minimize the total surface energy [16]. They also tend to migrate towards the edge from where they eventually escape the interface, thereby lowering the overall density of bubbles. Figure 3(d) is an AFM map of the same region as figure 3(c) after 3 h vacuum annealing at 200 °C exhibiting a complete removal of wrinkles and a remarkable reduction in bubbles. The higher resolution AFM map in figure 3(e) of the red-outlined region features a nearly pristine surface with a clean step of 7.2 Å (figure 3(f)) and a surface roughness of ±1.4 Å (rms) over the entire flake. This is in striking contrast to the MoS_2 flake transferred from untreated PDMS where the surface quality remained compromised by PDMS residues even after prolonged annealing as shown in figures 2(b), (c). The corresponding AFM phase map in figure 3(f) (inset) shows a clear phase contrast between MoS_2 and hBN (unlike figure 1(g)) providing further evidence for the decrease in residues by UV-O_3 treatment of PDMS. Detailed AFM analysis of two additional 1L-MoS_2 flakes transferred from UV-O_3 treated PDMS can be found in supplementary figures S3–S4 showing similarly clean surfaces.

Thus our recipe provides a new method to obtain very clean 2D material flakes on hBN. We would like to stress that a combination of UV-O_3 pre-cleaning followed by vacuum annealing is crucial, and vacuum annealing by itself does not result in a pristine surface as evident from figure 2. Note that here we transferred MoS_2 onto atomically smooth hBN flakes to decouple the SiO_2 substrate roughness from the surface topography of MoS_2 which allowed us to better resolve surface residues using AFM. Although the surface cleanliness does not depend on the substrate used, we have observed that the removal of bubbles and wrinkles during vacuum annealing is not very effective for MoS_2 transferred directly on SiO_2 (see discussion in supplementary section S4).

3. Optical characterization

To further characterize the effect of PDMS transfer on the optical properties of MoS_2, we performed PL and Raman spectroscopy. Experimental details can be found in section 5 (methods). Spatial maps of the spectrally integrated PL counts were recorded from the MoS_2 flake in figure 1(d) transferred

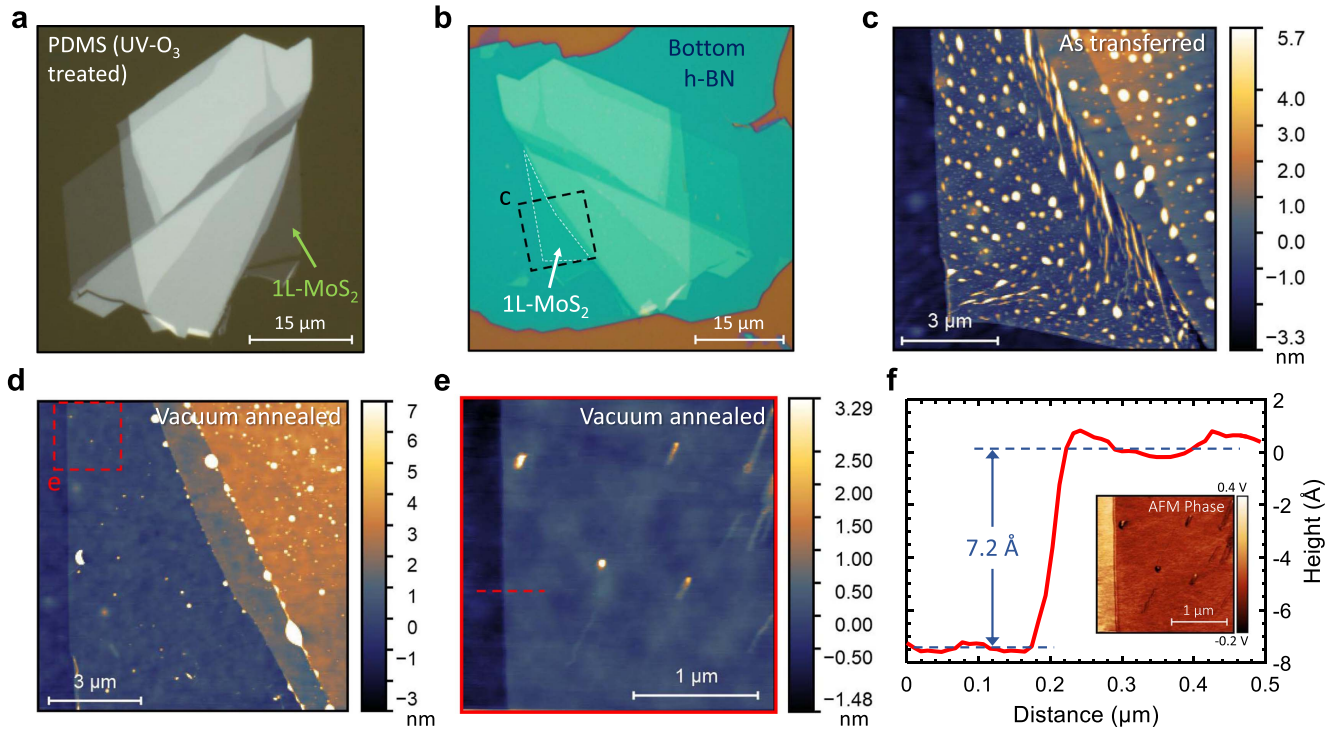

Figure 3. Clean transfer from UV-ozone cleaned PDMS. (a) Optical microscope image of 1L-MoS_2 exfoliated on 30 min UV-O_3 cleaned PDMS. (b) The same MoS_2 flake after transfer to hBN with the monolayer segment demarcated. (c) AFM topography map of the region outlined in (b). Areas densely covered with residues like in figures 1(e) or (f) could no longer be detected although a considerable amount of bubbles do occur which could also be efficiently removed. (d) AFM map of the same region showing a drastic reduction in bubbles and wrinkles from the entire flake after 200 °C vacuum annealing. (e) Higher resolution AFM map of the red-outlined region in (d) displaying a very clean and smooth MoS_2 surface. The faint streaks correspond to migration paths of residual bubbles which could not reach the MoS_2 edge and get released. (f) Height profile along the red-dashed line in (e) exhibiting a clear monolayer MoS_2 step of 7.2 Å unlike in figures 1(h) or 2(b), (c). Inset: AFM phase map recorded together with the topography in (e) revealing a clear phase contrast between MoS_2 and hBN which further indicates the absence of residues (compare with figure 1(g)).

using untreated PDMS (labelled as 'untreated' in figure 4) as well as from the clean MoS_2 flake transferred using UV-O_3 treated PDMS and subsequently vacuum annealed (figure 3(d)). PL maps of the two flakes depicted in figures 4(a), (b) show no apparent differences and the count rates were comparable for similar excitation powers. This indicates that PDMS residues (and/or vacuum annealing) do not seem to affect the overall PL quantum yield which could be one reason why residues have been overlooked in the past. The PL spectra of the two flakes, however, did show some interesting differences.

Besides the well-known A, B-exciton and trion (X^-) peaks, a new broad feature around 1.68 eV can be noticed in figure 4(c) in the PL spectra of untreated MoS_2. This low-energy peak can be better visualized at the locations marked by green and yellow dots in figure 4(a) where thick PDMS layers were present on MoS_2 (as shown previously in the AFM map in figure 1(f)). At these spots, the main excitonic peaks were weaker which made it easier to resolve the new peak (see figure 4(c) inset). Surprisingly, this peak could not be detected in MoS_2 flakes transferred from UV-O_3 treated PDMS (light blue and orange curves in figure 4(d) inset) as well as in the fluorescence spectra of an untreated PDMS stamp without MoS_2 (data not shown here). It appeared in the PL spectra of MoS_2 only when PDMS residues were present on MoS_2 but its true origin is unclear at present. Such a broad low-energy emission could possibly be attributed to impurity bound excitons at room temperature [33, 42] whose creation, however, is still not well understood in literature and a more detailed investigation is needed to elucidate the exact mechanism that gives rise to this additional peak.

Apart from this, it can be clearly observed in figure 4(d) that the A-exciton peaks of as-transferred MoS_2 (light and dark blue curves) are slightly blue-shifted with respect to that of vacuum annealed MoS_2 (orange curve) and lie at 1.887 ± 0.002 eV which agrees very well with the value of 1.89 eV measured previously on MoS_2 transferred from PDMS onto various substrates [43]. On the contrary, for vacuum annealed MoS_2 the A-exciton peak lies at 1.876 ± 0.002 eV, very close to that of MoS_2 exfoliated directly on SiO_2 [44, 45]. By comparing the PL spectra at various locations on the two flakes in figures 4(a), (b) and performing multi-Lorentzian fitting to decouple the trion peak from the exciton peak, we estimated a blue-shift of 11 ± 3 meV for the A-exciton peak of as-transferred MoS_2. Moreover, one can also notice a blue-shift in the B-exciton peak as highlighted by the Lorentzian fits in figure 4(e). The complete set of fits for the entire spectra can be found in supplementary figure S6.

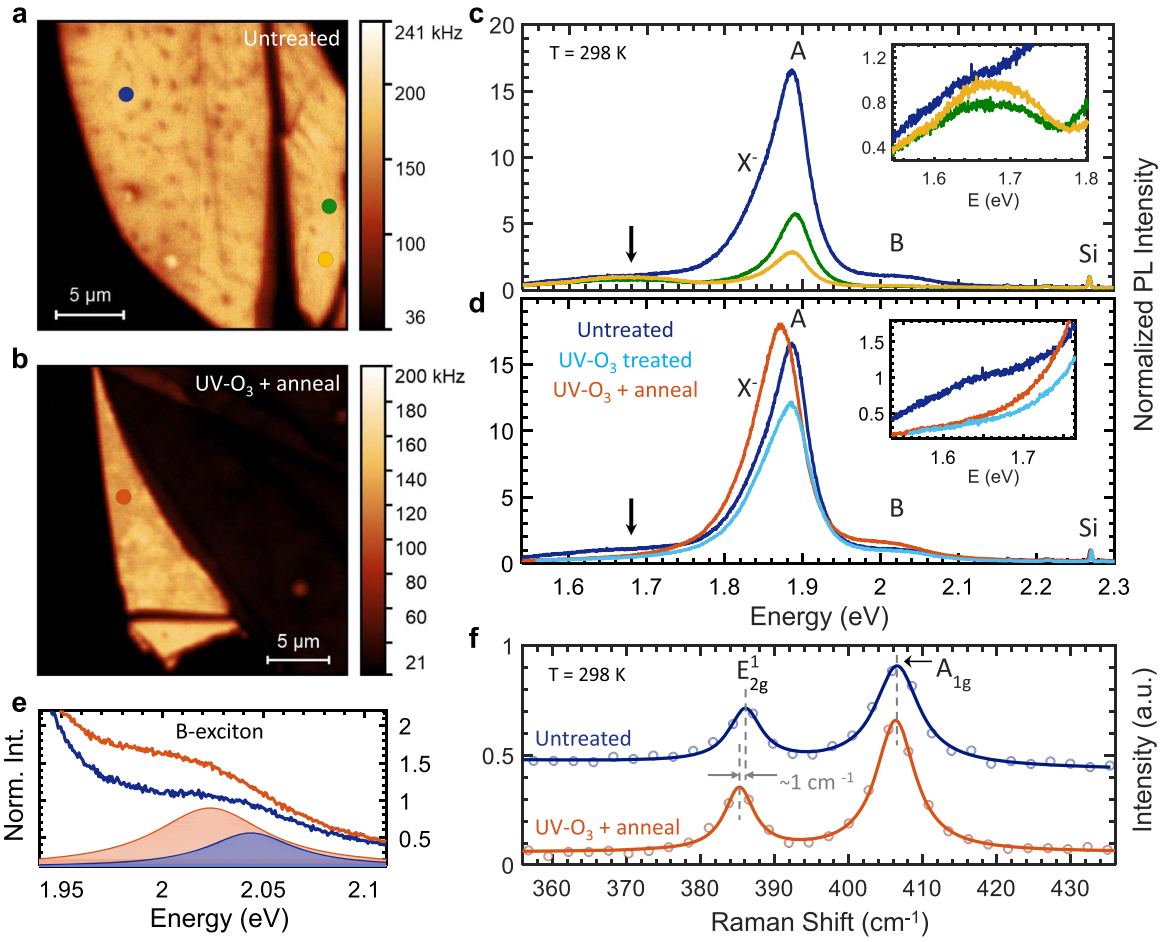

Figure 4. Optical characterization. (a, b) Spatial maps of the spectrally integrated PL counts from the 1L-MoS_2 flakes in figures 1(d), 3(d) displaying similar emission intensities. The dark spots and lines in (a) are interfacial bubbles and wrinkles respectively (see figure 1(d)) where the photon counts were somewhat decreased. (c) PL spectra of MoS_2 transferred from untreated PDMS recorded at points marked by matching colored dots in (a). Besides the indicated excitonic peaks, all spectra also show a low-energy feature (marked by arrow) around 1.68 eV. (d) PL spectra of MoS_2 transferred from UV-O_3 treated PDMS showing the absence of any low-energy feature in comparison with MoS_2 from untreated PDMS. This indicates that the new feature arises only in the presence of PDMS residues on MoS_2. Apart from this, the PL spectra in light and dark blue show blue-shifted A, B excitonic peaks which reveals the presence of compressive strain in as-transferred MoS_2 (irrespective of PDMS pre-treatment). This strain got released from the flake in (b) upon annealing. The PL spectra in light blue was recorded from the flake in figure S3a before annealing while the annealed MoS_2 spectra (orange) was taken from the flake in (b). Insets: magnified plots of the spectra around 1.68 eV. (e) A magnified view of the B-exciton emission in (d). The filled area plots are Lorentzian fits to the B-exciton peaks and display a clear shift in the center positions. (f) Raman spectra of the two flakes (vertically offset for clarity). The empty circles are measured data points while the smooth lines are Lorentzian fits to estimate the center position of each peak. The E^1_{2g} peak (in blue) is up-shifted by $\sim$1 cm^{-1} which also indicates a build-up of compressive strain in as-transferred MoS_2, in agreement with the PL spectra. All spectra have been normalized to the Raman peak of silicon for a better comparison.

In order to understand the origin of the A, B-exciton blue-shift upon transfer, we performed Raman spectroscopy to gain further insight from the E^1_{2g} mode which is sensitive to strain in MoS_2. In exfoliated, unstrained 1L-MoS_2 at room temperature, the E^1_{2g} peak should lie at 385 cm^{-1} [46] whereas for our as-transferred MoS_2 on hBN it lies at $\sim$386 cm^{-1} (blue curve in figure 4(f)). An E^1_{2g} peak up-shift signifies an increase in built-in compressive strain, thus implying that PDMS not only leaves residues behind, but can also compress the MoS_2 during transfer. An up-shift of $\sim$1 cm^{-1} corresponds to an accumulation of $\sim$0.22% compressive strain in MoS_2 after transfer [47], similar to estimate made by Buscema *et al* [43]. This induced strain causes an increase in the direct bandgap at the *K*-point which leads to blue-shifted A, B-exciton emission [48, 49]. According to previously reported DFT calculations [50] as well as experimental results [47], a 0.22% strain would induce an A-exciton shift of 10 ± 1.5 meV which is in good agreement with the shift of 11 ± 3 meV estimated from our PL measurements. For the sake of completeness, one can also compare the A_{1g} peaks in the two Raman spectra to characterize the effect of residues on doping. The strong electron–phonon coupling of the out-of-plane A_{1g} mode in MoS_2 causes it to down-shift with increasing doping [51]. In figure 4f, the two A_{1g} peaks lying at $\sim$406.5 cm^{-1} imply a low n-doping in both MoS_2 flakes on hBN (compared to 403–404 cm^{-1} for 1L-MoS_2 on SiO_2) [43, 46].

The origin of strain can possibly be attributed to the inherent lack of stiffness of PDMS. As discussed previously

by Gomez *et al* [18], PDMS being soft can get slightly deformed during transfer by the pressure exerted on PDMS upon coming in contact with the target substrate. It is quite likely that this deformation of PDMS induces a compressive strain in the flake being transferred as measured for MoS_2 in our case. The induced strain eventually gets released upon vacuum annealing, down-shifting the E^1_{2g} peak to 385 cm^{-1} and at the same time red-shifting the A, B-exciton peaks to unstrained values close to that of directly exfoliated MoS_2. The release of transfer induced compression in MoS_2 can also be evidenced in the AFM scans in figures 3(c), (d) before and after annealing where an increase in the total surface area upon annealing can be clearly noticed.

4. Conclusions

To summarize, we have demonstrated that PDMS residues as well as compressive strain can be present in 2D materials exfoliated onto and transferred from PDMS stamps. Using 1L-MoS_2 as an example, we have observed evidence of surface contamination in both AFM maps and PL spectra. UV-O_3 treatment of PDMS prior to exfoliation significantly reduces the amount of unwanted surface oligomers which results in a cleaner transfer of MoS_2 in comparison with untreated PDMS. We showed that a 1L-MoS_2 surface of a very high-quality can be obtained by a combination of UV-O_3 pre-cleaning followed by vacuum annealing after transfer. AFM topography of annealed MoS_2 flakes on hBN displayed a homogeneously smooth surface with a substantial reduction in interfacial bubbles and wrinkles. PL spectroscopy of as-transferred MoS_2 revealed blue-shifted A, B-exciton peaks due to an accumulation of compressive strain during the transfer. This induced compression could be released by a post-transfer vacuum anneal.

It is advantageous to exfoliate MoS_2 on PDMS for obtaining large area (>1000 μm^2) monolayer MoS_2 flakes with a high yield unlike direct exfoliation on SiO_2 which results in relatively smaller flakes. The recipe we provided now makes it possible to integrate these large area flakes exfoliated on PDMS into clean heterostructures for high performance electronic and photonic devices. Our results are valuable for future experimental studies and practical applications utilizing clean 2D material heterostructures.

One must keep in mind that even though PDMS residues do not significantly influence the optical properties of MoS_2, surface residues could still affect electrical transport by scattering charge carriers and thereby reduce carrier mobility. Moreover, trapped residues within TMDC heterostructures could also weaken interlayer coupling [31] and adversely affect physical phenomena such as interlayer charge recombination or separation, interlayer electron–phonon coupling, polariton formation, out-of-plane tunneling, etc., which rely on high-quality interfaces. Hence, the importance of eliminating residues while stacking 2D materials using PDMS, or any other technique in general, cannot be overstated. In this direction, our results highlight the significance of a careful characterization and optimization of any transfer procedure and subsequent processing steps in order to preserve interface quality and obtain unperturbed crystal structures with well-defined physical properties.

5. Methods

All transfers were done with a SÜSS MicroTec MJB4 mask aligner in air. Annealing was performed in a quartz tube furnace (Carbolite Gero) at 200 °C for 3 h in a low vacuum of 5×10^{-3} mbar (limited by our rotary pump). Before heating, the quartz tube was flushed several times with argon gas to remove any residual water or oxygen molecules. After 3 h, the furnace was left for a few hours to cool down naturally to room temperature before taking out the samples.

All measurements were carried out at room temperature under ambient conditions. For PL measurements, samples were mounted on a piezoelectric stage and excited with a 532 nm Nd:YAG laser (attenuated to 15 μW power) using a 50x air objective (0.8 NA) in a scanning confocal microscopy setup. The MoS_2 flakes were raster scanned across the laser focus and photon counts at each xy-position were recorded with a single photon counting module (Perkin Elmer SPCM-AQRH-14) after passing through a 532 nm RazorEdge long-pass filter. PL spectra were measured with a Princeton Instruments Acton SP300i spectrometer at 100 μW excitation power (30 s integration). For Raman spectroscopy, excitation was done with the 530.8 nm line of an Ar-Kr laser (Coherent) at 100 μW power and the back-scattered light was dispersed onto a grating with 1200 grooves mm^{-1}. The grating was calibrated with a Neon lamp before recording the Raman spectra. Lorentzian fits were obtained using the freely available *peak-o-mat* software [52]. All spectra were normalized to the Raman peak of p^+Si lying at 521.7 cm^{-1} for a better comparison.

Acknowledgments

This research was supported by the Swiss National Science Foundation (grant no. 200021_165841) and ETH Zürich (ETH-32 15-1). TT and KW acknowledge support from the Elemental Strategy Initiative conducted by the MEXT, Japan and JSPS KAKENHI (grant no. JP15K21722).

Author contributions

The overall project was conceived and supervised by PB and LN. AJ developed the cleaning procedure, fabricated the samples, performed the measurements and wrote the manuscript. PB built the confocal optical microscopy setup used for PL spectroscopy of MoS_2. Raman characterization was carried out together with SH. The vacuum tube furnace was setup by MP who also wrote the LabVIEW script for performing vacuum annealing. TT and KW synthesized the hBN crystals used in this study. PB, SH, MP and LN also

participated in discussion of results and contributed to writing the manuscript.

ORCID iDs

Achint Jain https://orcid.org/0000-0002-3495-5935
Palash Bharadwaj https://orcid.org/0000-0003-0722-6697
Sebastian Heeg https://orcid.org/0000-0002-6485-3083
Markus Parzefall https://orcid.org/0000-0003-2930-6698
Lukas Novotny https://orcid.org/0000-0002-9970-8345

References

[1] Xu M, Liang T, Shi M and Chen H 2013 Graphene-like two-dimensional materials *Chem. Rev.* **113** 3766–98
[2] Bhimanapati G R *et al* 2015 Recent advances in two-dimensional materials beyond graphene *ACS Nano* **9** 11509–39
[3] Geim A K and Grigorieva I V 2013 Van der Waals heterostructures *Nature* **499** 419–25
[4] Novoselov K, Mishchenko A, Carvalho A and Neto A C 2016 2D materials and van der Waals heterostructures *Science* **353** 461
[5] Lim H, Yoon S I, Kim G, Jang A-R and Shin H S 2014 Stacking of two-dimensional materials in lateral and vertical directions *Chem. Mater.* **26** 4891–903
[6] Gong Y *et al* 2014 Vertical and in-plane heterostructures from WS_2/MoS_2 monolayers *Nat. Mater.* **13** 1135–42
[7] Koma A, Sunouchi K and Miyajima T 1985 Fabrication of ultrathin heterostructures with van der Waals epitaxy *J. Vac Sci. Technol.* B **3** 724
[8] Lin Y-C *et al* 2015 Atomically thin resonant tunnel diodes built from synthetic van der Waals heterostructures *Nat. Commun.* **6** 7311
[9] McManus D *et al* 2017 Water-based and biocompatible 2D crystal inks for all-inkjet-printed heterostructures *Nat. Nanotechnol.* **12** 343–50
[10] Dean C R *et al* 2010 Boron nitride substrates for high-quality graphene electronics *Nat. Nanotechnol.* **5** 722–6
[11] Wang L *et al* 2013 One-dimensional electrical contact to a two-dimensional material *Science* **342** 614–7
[12] Zomer P J, Guimarães M H D, Brant J C, Tombros N and van Wees B J 2014 Fast pick up technique for high quality heterostructures of bilayer graphene and hexagonal boron nitride *Appl. Phys. Lett.* **105** 013101
[13] Kretinin A V *et al* 2014 Electronic properties of graphene encapsulated with different two-dimensional atomic crystals *Nano Lett.* **14** 3270–6
[14] Parzefall M *et al* 2015 Antenna-coupled photon emission from hexagonal boron nitride tunnel junctions *Nat. Nanotechnol.* **10** 1058–63
[15] Pizzocchero F *et al* 2016 The hot pick-up technique for batch assembly of van der Waals heterostructures *Nat. Commun.* **7** 11894
[16] Frisenda R *et al* 2018 Recent progress in the assembly of nanodevices and van der Waals heterostructures by deterministic placement of 2D materials *Chem. Soc. Rev.* **47** 53–68
[17] Meitl M A *et al* 2006 Transfer printing by kinetic control of adhesion to an elastomeric stamp *Nat. Mater.* **5** 33–8
[18] Castellanos-Gomez A *et al* 2014 Deterministic transfer of two-dimensional materials by all-dry viscoelastic stamping *2D Mater.* **1** 011002
[19] Kumar A and Whitesides G M 1993 Features of gold having micrometer to centimeter dimensions can be formed through a combination of stamping with an elastomeric stamp and an alkanethiol ink followed by chemical etching *Appl. Phys. Lett.* **63** 2002–4
[20] Duffy D C, McDonald J C, Schueller O J A and Whitesides G M 1998 Rapid prototyping of microfluidic systems in poly(dimethylsiloxane) *Anal. Chem.* **70** 4974–84
[21] Rogers J A, Someya T and Huang Y 2010 Materials and mechanics for stretchable electronics *Science* **327** 1603–7
[22] Xia Y and Whitesides G M 1998 Soft lithography *Angew. Chem., Int. Ed. Engl.* **37** 550–75
[23] Regehr K J *et al* 2009 Biological implications of polydimethylsiloxane-based microfluidic cell culture *Lab Chip* **9** 2132–9
[24] Lee J N, Park C and Whitesides G M 2003 Solvent compatibility of poly(dimethylsiloxane)-based microfluidic devices *Anal. Chem.* **75** 6544–54
[25] Glasmästar K, Gold J, Andersson A-S, Sutherland D S and Kasemo B 2003 Silicone transfer during microcontact printing *Langmuir* **19** 5475–83
[26] Briseno A L *et al* 2006 Patterning organic semiconductors using dry poly(dimethylsiloxane) elastomeric stamps for thin film transistors *J. Am. Chem. Soc.* **128** 3880–1
[27] Böhm I, Lampert A, Buck M, Eisert F and Grunze M 1999 A spectroscopic study of thiol layers prepared by contact printing *Appl. Surf. Sci.* **141** 237–43
[28] Yunus S, de Looringhe C d C, Poleunis C and Delcorte A 2007 Diffusion of oligomers from polydimethylsiloxane stamps in microcontact printing: surface analysis and possible application *Surf. Int. Anal.* **39** 922–5
[29] Allen M J *et al* 2009 Soft transfer printing of chemically converted graphene *Adv. Mat.* **21** 2098–102
[30] Liu K *et al* 2014 Elastic properties of chemical-vapor-deposited monolayer MoS_2, WS_2, and their bilayer heterostructures *Nano Lett.* **14** 5097–103
[31] Tongay S *et al* 2014 Tuning interlayer coupling in large-area heterostructures with CVD-grown MoS_2 and WS_2 monolayers *Nano Lett.* **14** 3185–90
[32] Tongay S *et al* 2013 Broad-range modulation of light emission in two-dimensional semiconductors by molecular physisorption gating *Nano Lett.* **13** 2831–6
[33] Tongay S *et al* 2013 Defects activated photoluminescence in two-dimensional semiconductors: interplay between bound, charged, and free excitons *Sci. Rep.* **3** 2657
[34] Yang L *et al* 2014 Chloride molecular doping technique on 2D materials: WS_2 and MoS_2 *Nano Lett.* **14** 6275–80
[35] Ouyang M, Yuan C, Muisener R J, Boulares A and Koberstein J T 2000 Conversion of some siloxane polymers to silicon oxide by UV/ozone photochemical processes *Chem. Mater.* **12** 1591–6
[36] Bodas D and Khan-Malek C 2007 Hydrophilization and hydrophobic recovery of PDMS by oxygen plasma and chemical treatment - an SEM investigation *Sensors Actuators* B **123** 368–73
[37] Morent R *et al* 2007 Adhesion enhancement by a dielectric barrier discharge of PDMS used for flexible and stretchable electronics *J. Phys. D: Appl. Phys.* **40** 7392–401
[38] Haigh S J *et al* 2012 Cross-sectional imaging of individual layers and buried interfaces of graphene-based heterostructures and superlattices *Nat. Mater.* **11** 764–7
[39] Cao Y *et al* 2015 Quality heterostructures from two-dimensional crystals unstable in air by their assembly in inert atmosphere *Nano Lett.* **15** 4914–21
[40] Kang K *et al* 2017 Layer-by-layer assembly of two-dimensional materials into wafer-scale heterostructures *Nature* **550** 229–33

[41] Wierzbowski J *et al* 2017 Direct exciton emission from atomically thin transition metal dichalcogenide heterostructures near the lifetime limit *Sci. Rep.* **7** 12383
[42] Chow P K *et al* 2015 Defect-induced photoluminescence in monolayer semiconducting transition metal dichalcogenides *ACS Nano* **9** 1520–7
[43] Buscema M, Steele G A, van der Zant H S J and Castellanos-Gomez A 2014 The effect of the substrate on the Raman and photoluminescence emission of single-layer MoS_2 *Nano Res.* **7** 561–71
[44] Schuller J A *et al* 2013 Orientation of luminescent excitons in layered nanomaterials *Nat. Nanotechnol.* **8** 271–6
[45] Amani M *et al* 2015 Near-unity photoluminescence quantum yield in MoS_2 *Science* **350** 1065–8
[46] Li H *et al* 2012 From bulk to monolayer MoS_2: evolution of raman scattering *Adv. Funct. Mater.* **22** 1385–90
[47] Conley H J *et al* 2013 Bandgap engineering of strained monolayer and bilayer MoS_2 *Nano Lett.* **13** 3626–30
[48] Nayak A P *et al* 2015 Pressure-dependent optical and vibrational properties of monolayer molybdenum disulfide *Nano Lett.* **15** 346–53
[49] Dou X, Ding K, Jiang D, Fan X and Sun B 2016 Probing spin–orbit coupling and interlayer coupling in atomically thin molybdenum disulfide using hydrostatic pressure *ACS Nano* **10** 1619–24
[50] Liu Z *et al* 2014 Strain and structure heterogeneity in MoS_2 atomic layers grown by chemical vapour deposition *Nat. Commun.* **5** 5246
[51] Chakraborty B *et al* 2012 Symmetry-dependent phonon renormalization in monolayer MoS_2 transistor *Phys. Rev.* B **85** 161403
[52] peak-o-mat http://lorentz.sourceforge.net/